RAD Conference Proceedings, vol. 6, pp. 31–37, 2022
ISSN 2466-4626 (online) | doi: 10.21175/RadProc.2022.06
www.rad-proceedings.org

ISO 4037 2019: ESTABLISHMENT OF X-RAY NARROW-SPECTRUM SERIES USED IN THE NATIONAL SECONDARY STANDARD DOSIMETRY LABORATORY OF MOROCCO

Omaima Essaad Belhaj[1*], Hamid Boukhal[1], El Mahjoub Chakir[2], Khaoula Laazouzi[1], Maryam Hadouachi[1], Younes Sadeq[2,3], Siham Belhaj[4], Meryem Bellahsaouia[2], Said Soudjay[5]

[1]RSN, Faculty of Sciences, University Abdelmalek Essaadi, Tetouan, Morocco
[2]LPMS, Faculty of Sciences, Ibn Tofail University, Kenitra, Morocco
[3]SSDL, National Center of Radiation Protection (CNRP), Ministry of Health, Sale, Morocco
[4]ENA, Marrakech, Morocco
[5]Faculty of Sciences, University of Comoros, Moroni, Comoros

Abstract. *The radiation qualities of the narrow-spectrum X-ray series in the range from 30 to 300 kV designed for calibration of radiation protection and dosimeter irradiation instruments have been established, characterized and validated experimentally in accordance with the recommendations of ISO4037-1:2019 in the automated X-ray calibration facility of the Service of Calibration and Metrology of Ionizing Radiation of a national Secondary Standard Dosimetry Laboratory (SSDL) in Morocco. The variety of the first half-value layer (1st HVL) and the second HVL (2nd HVL) between the experimental results and the values given in ISO 4037-1:2019 were all within 10%; similarly, the homogeneity coefficients h were between 0.88 and 1.0 according to ISO 4037:2019. In addition, the Monte Carlo code Gamos/Geant4 was used to simulate the spectra of these radiation qualities, which showed good agreement with the spectra given in ISO 4037-1 and with the results found by the SpekPy and SpekCalc software. For the conversion coefficients the highest difference between values determined through experiment and those established by ISO 4037-3 were 5.5 %. The study and characterization of the reference radiations of the narrow spectrum series in the national secondary standard dosimetry laboratory of Morocco revealed a good conformity to the recommendations of the ISO 4037:2019.*

Keywords: *half-value layer, narrow-spectrum series, Monte Carlo, SSDL, radiation protection*

1. INTRODUCTION

To ensure that the tests and calibration of radiation protection instruments, namely dosimeters and dose rate meters and the determination of their response, are carried out in a reliable and traceable manner, it is necessary to use reference radiation fields and, for this purpose and the standardization between different organizations, the international standard revised and deleted the technical specification series ISO 4037 1996, and made available ISO4037-1:2019 [1], ISO4037-2:2019 [2], ISO4037-3:2019 [3] and ISO4037-4:2019 [4].

It is very important to establish the radiation reference series based on the recommendations of ISO4037-1:2019 at the National Center for Radiation Protection in Morocco which is one of the members of the IAEA/WHO SSDL network.

In this paper, the narrow spectrum series of X-rays going from 30 kVp to 300 kVp was established according to the above standards, inherent filtration of the tube, supplementary filtration, first half-value layer (1st HVL), second half-value layer (2nd HVL) and homogeneity coefficient were measured experimentally.

These X-ray beams are named by N-***, where *** represents the high voltage, in kilovolts, applied to the X-ray generator.

Measuring such a spectrum for these X-ray beams can be both time consuming and difficult, especially when large corrections must be applied to the measured pulse height distributions of the observed spectra [5]. For this reason, Monte Carlo method was used to simulate the energy spectrum of this series utilizing the Gamos/Geant4 while calculating the average energy and comparing the resolution with the standard technical specifications.

2. MATERIALS AND METHODS

2.1. Equipment

2.1.1. The X-ray beam irradiator

The X-ray calibration system supplied is able to produce radiation beam qualities for calibration of dosimetry equipment per ISO-4037 requirements.

The measurements were carried out with a machine model X80-320 of X-ray irradiator represented by HOPEWELL DESIGNS, INC and that represents a complete system for the irradiation of the badges of dosimetry of the personnel and the instruments of detection of the radiations with X-rays. It possesses ceramic tube and an anode target in tungsten with an angle of 20°, a focal field of 5.5 mm and an inherent filtration of 3 mm of beryllium. The high voltage that

* omaimaessaad.belhaj@gmail.com

may be applied to this X-ray tube varies from 15 to 320 kVp, a current of 0.5 mA to 13 mA and a minimum power of 1500 W to 4200 W. The charge generated by the X-ray photons was measured using a PS (50) ionization chamber and read from an associated PTW electrometer Unidos Webline T10023.

The principal subsystems of the X-ray system are: 1) the shielded enclosure, 2) filter wheel, 3) the beam shutter and collimator, 4) monitor chamber, 5) added filtration, 6) HVL support, 7) ionization chamber.

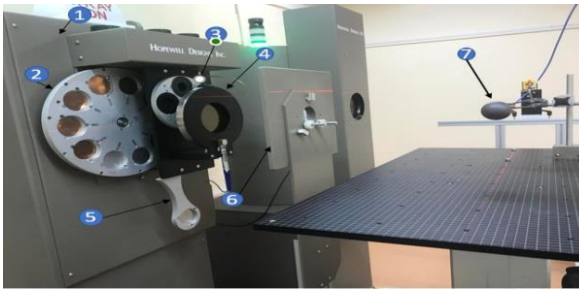

Figure 1. Set-up of the X-ray beam irradiator used in the SSDL Model X80-320 kV for HVL's determination.

2.1.2. Transmission monitor chamber

Large size plane-parallel transmission monitor chamber type 34014 for use as dose monitors combined with calibration facilities designed by PTW FREIBURG is placed beyond the X-ray collimators for an accurate reading of dose area product.

The sensitive volumes are designed as twin chambers with 2.5 mm measuring depth each and diameter of 148 mm.

A monitor chamber shall be used in order to permit application of corrections for fluctuations in the air kerma rate [1].

2.1.3. Ionization chamber

The spherical ionization chamber PS (50) TN32007 SN 000007 with a nominal volume of 50 cm^3 is used as the secondary standard for radiation protection. The spherical structure of the ionization chamber provides a nearly uniform response to radiation from all directions. The ionization chamber must be stable over time, centered and aligned with the beam axis.

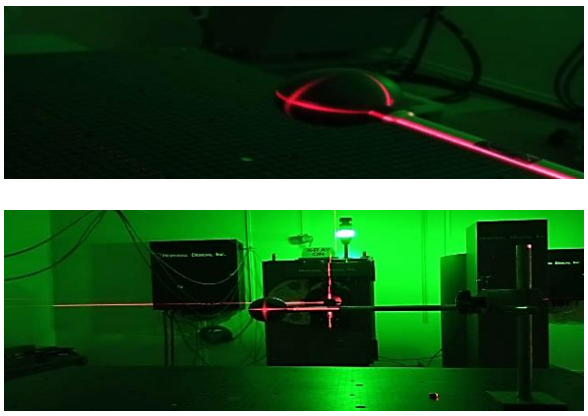

Figure 2. Ionization chamber alignment

During measurement, the Kerma values in air and the charge collected from the ionization chamber PS (50) are multiplied by a correction factor for temperature and pressure calculated for the measured values of temperature and pressure.

2.1.4. Metal - Attenuator-

The metal absorbers copper and Aluminum used in this work have a purity higher than 99.98 %.

2.2. Measurement procedure

2.2.1. Beam profile

In order for the beam shaping to be effective, it is necessary before establishing any radiation quality to measure the homogeneity of the beam to make sure that the ionization chamber is fully irradiated.

At a distance of 50 cm from the tube, the measurement of the horizontal and vertical profile of the beam was carried out.

2.2.2. Inherent filtration

The X-ray beam is filtered at the exit of the tube by an inherent filtration caused by the insulating glass envelope, and the sheath window, and an additional filtration, which have for objective to reduce the intensity of the X-ray, and to increase the energy (the low energies will be absorbed in priority with the filtration, which involves an augmentation of the average energy of the beam). So, the inherent filtration is characteristic of an X-ray tube and it cannot be changed.

Without any additional filtration and at 60 kV and the tube current of 10 mA, the inherent filtration was established using the ionization chamber Ps (50) placed at 1m from the tube center. Aluminum filters with different thicknesses were added/ superimposed in the beam in order to calculate the HVL taking the 1st value in absence of filter as reference.

The determination method consists of 10 intensity readings of 60 seconds each, performed with a superposition of additional aluminum filters placed in such a manner as to obtain a reduction of about 50% of the initial intensity. The inherent filtration was obtained by an extrapolation curve generated from the data in table 9 of the ISO4037-1 standard [1].

Of the fact that the total filtration = inherent filtration + additional filtration and after determining the inherent filtration, the additional filtration was deduced.

The determination method used for the determination of inherent filtration is in conformity with ISO 4037 [1] and ICRU report 10b [6].

2.2.3. Half-value layer measurement

The 1st half-attenuation layer is described in ISO 4037 as the thickness of the specific material that attenuates the radiation beam to a measurement of one half of its initial value, while the 2nd half-attenuation layer is described as the thickness of the same material for the measurement of the 1st half-attenuation layer that attenuates the beam to a measurement of one

quarter of its initial value minus the 1st half attenuation layer. For homogeneity it is the ratio of 1st HVL and 2nd HVL. In the presence of inherent filtration, and using different thicknesses of copper or Al filters, HVL's measurements of different radiation qualities N-30, N-40, N-60, N-80, N-100, N-120, N-150, N-200, N-250, N-300 were performed according to ISO4037:2019.

The HVL measurement procedure is performed either by determining the attenuation curves or by using interpolation for the determination of 1s tHVL and 2nd HVL while taking the 1st measurement in the absence of a filter as reference values which correspond to 100%.

The results found experimentally for the HVL's were compared with the results of the SpekCalc [7-9] and SpekPy version 2.0.7 [10-18] software.

2.2.4. X-ray spectra

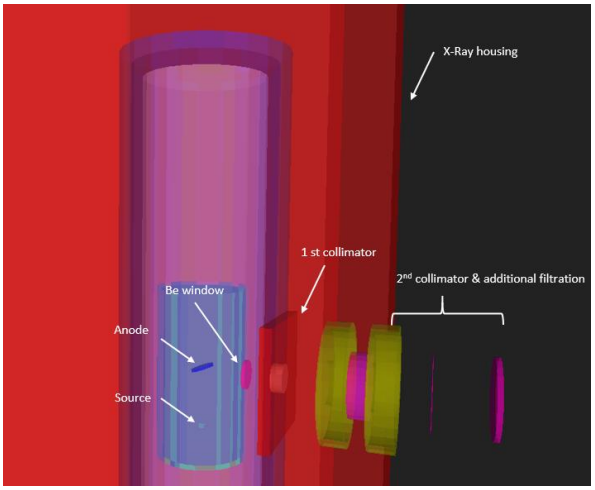

Figure 3. Simplified geometry of simulated X-ray generator using GAMOS/GEANT4

The energy spectrum of the radiation quality is one of the important elements to characterize the radiation quality. Since the measurement procedure is delicate, time consuming and requires a lot of correction, Monte Carlo simulation is employed. Monte Carlo methods are widely used, especially to solve radiation transport problems. Many general-purpose Monte Carlo (MC) codes that can facilitate the experiment and minimize the time to process the phenomena [19,20] have been developed, such as EGSnrc [21], EGS4/EGSnrc [22,23], ETRAN [24], MCNP [25], PENELOPE [26], Fluka [27] and Gamos [19, 28].

To make a simulation with Gamos/Geant4 the minimum to define is the geometry, the primary generator (initial particles), the physics list, and the format of the output which is mainly obtained by the user actions, the sensitive detectors, or the scorer.

In this paper, the Gamos/Geant4 version 6.2.0 Monte Carlo code was utilized to simulate the spectra of the radiation qualities included in the ISO 4037-1 series of narrow spectra using write and summation of phase space files (RTGeneratorPhaseSpace/SumPS). An accelerated electron strikes the anode target at an angle of 22° to start the simulation. The primary particle (the initial) is moved a distance S (mean free path) until the next interaction, at which point all the particles involved with their data are stored in phase space file and moved again. This procedure is continued until the simulated particle's energy falls below a preset cut-off energy, or it exits the region of interest or the system entirely. By observing the histograms at each phase space file, one can understand how the particles are transported along their trajectories.

In our case the creation of the geometry file (.geom), and the input data file (.in) was based on the documentation of the tutorial and the solution code in the GAMOS installation, in the directory GAMOS.6.2.0/tutorials/XRayTutorial with using GmEMPhysics list and bremsstrahlung splitting. We used a random seed to speed up this simulation.

From the spectral distribution data, the average energy can be derived from the X-ray qualities, which is defined by the following relation:

$$\bar{E} = \frac{\int_0^{Emax} \phi(E) E dE}{\int_0^{Emax} \phi(E) dE} \qquad (1)$$

In addition to the determination of the spectral characteristics by the Monte Carlo method using the Gamos/Geant4 code, the SpekCalc and SpekPy software mentioned above were used for the validation.

2.2.5. Conversion coefficients

From a practical point of view, the issue is to connect the operational quantities to physical reference quantities that can be measured with appropriate by means of appropriate equipment whether of a radiometric nature or in reference to the action of radiation on matter, therefore of a dosimetric nature [29] .The conversion coefficient Hp (10)/K_{air} which allows to determine the dose equivalent Hp(10) from the measured values of air kerma with the ionization chamber PS(50) described above and the measured values of Hp(10) with the parallel plate ionization chamber (Figure 4) which is a secondary standard ionization detector type 34035 [30] created at PTB Germany allowing the direct measurement of personal dose equivalent on a slab phantom.

The Hp (10) chamber's primary calibrated in the PTB laboratory characteristics are its 10 cm^3 measurement volume, 31x300x300 mm^3 measuring component dimensions, and 120x300x300 mm^3 slab phantom dimensions.

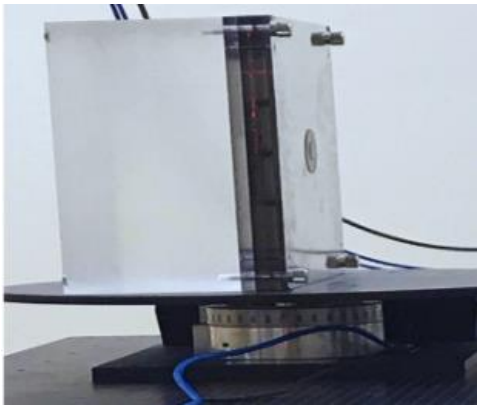

Figure 4. Parallel plat ionization chamber calibrated in the PTB laboratory

The kerma-to-personal dose equivalent Hp(10) conversion coefficient is defined as the ratio of the quantities Hp(10) and the air kerma K_{air}:

$$hpK(10;N, \alpha)_{slab}=Hp(10)/ K_{air} \quad (2)$$

where:

- N: narrow spectrum series
- α: angle of incidence (°)
- Hp(10):phantom related operational quantities
- K_{air}: the air kerma determined according to ISO 4037.

The conversion coefficients depend on the energy, the directional distribution of the incident radiation and also the phantom used in the calibration [31].

3.Results and Discussion

3.1. Beam profile

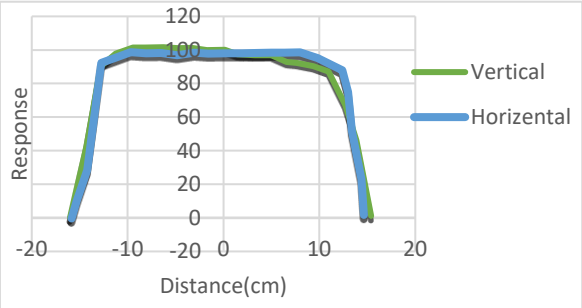

Figure 5. Measurement results of uniformity of radiation field

Figure 5 shows the vertical and horizontal profile of the R-X beam, the inclination of the vertical plate is due to the inclination of the anode. A homogeneous region with a diameter of 20 cm was obtained at a distance of 50 cm from the tube.

3.2. Inherent filtration

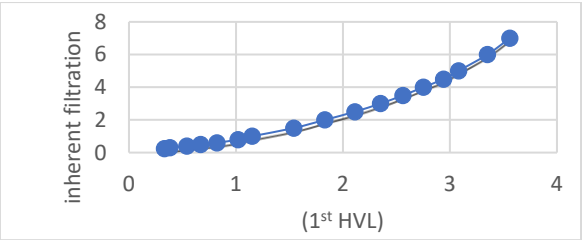

Figure 6. Inherent filtration according to the intensity from ISO standard

Table 1. Results of the inherent filtration

1st HVL (mm of Aluminum) 60 kV	0.38
Inherent Tube Filtration (mm of Aluminum)	0.29
Additional Inherent Filtration (mm of Aluminum)	3.70

Table 1 show the results for inherent filtration. The inherent filtration found is 0.29 mm Al for a half-value layer (HVL) of 0.38 mm Al. This value was obtained by an extrapolation curve generated from the data provided by Table 9 of ISO 4037-1. According to ISO 4037-1, additional filtration is equal to the total filtration (4 mm Al) less the inherent filtration of the tube.

3.3. Half-value layer measurement

Tables 2 and 3 represent the results found experimentally (SSDL) and the results found by SpekCalc and SpekPy. Concerning the beam qualities N-200, N-250, N-350, their additional filtration consists of lead filters, this material is not found in the library of materials of SpekCalc.

Table 2. Measurements results of 1st HVL's

Radiation quality (mm Al/Cu)	**Tube voltage (kV)**	**1st HVL (mm)**			
		ISO	***SSDL***	***Spek Calc***	***Spek Py***
N-30 (mm Al)	30	1.16	1.13	1.17	1.16
N-40 (mm Cu)	40	0.085	0.082	0.086	0.08
N-60 (mm Cu)	60	0.234	0.24	0.24	0.23
N-80 (mm Cu)	80	0.578	0.6	0.6	0.57
N-100 (mm Cu)	100	1.09	1.153	1.13	1.09
N-120 (mm Cu)	120	1.67	1.76	1.73	1.68
N-150 (mm Cu)	150	2.3	2.4	2.39	2.3
N-200 (mm Cu)	200	3.92	4.14	-	3.94
N-250 (mm Cu)	250	5.1	5.18	-	5.13
N-300 (mm Cu)	300	5.96	6.253	-	6.04

Table 3. Measurements results of 2nd HVL's.

Radiation quality (mm Al/Cu)	**2nd HVL (mm)**			
	ISO	***SSDL***	***SpekCalc***	***SpekPy***
N-30 (mm Al)	1.28	1.24	1.29	1.28
N-40 (mm Cu)	0.093	0.092	0.093	0.091
N-60 (mm Cu)	0.263	0.26	0.266	0.26
N-80 (mm Cu)	0.622	0.62	0.635	0.62
N-100 (mm Cu)	1.15	1.205	1.19	1.15
N-120 (mm Cu)	1.73	1.85	1.8	1.75
N-150 (mm Cu)	2.41	2.582	2.5	2.43
N-200(mm Cu)	3.99	4.25	-	4
N-250 (mm Cu)	5.14	5.1	-	5.18
N-300 (mm Cu)	6	6.37	-	6.07

Table 4. Measurements results of homogeneous coefficients

Radiation quality	**Tube voltage (kV)**	**homogeneous (%)**		
		SSDL	***SpekCalc***	***SpekPy***
N-30	30	91	91	91
N-40	40	89	91.8	91
N-60	60	92.3	89.2	89
N-80	80	96.8	92.9	93
N-100	100	95.7	95	94
N-120	120	95.1	96.4	96
N-150	150	94.8	95.4	95
N-200	200	97.4	-	98.3
N-250	250	89.2	-	99
N-300	300	98.1	-	99

Table 5. Deviation result of 1st HVL's

Radiation quality	ΔHVL1 (%)		
	SSDL	***SpekCalc***	***SpekPy***
N-30	2.65	0.86	0.000
N-40	3.66	0.59	2.353
N-60	2.50	1.28	0.855
N-80	3.67	2.08	0.554
N-100	5.46	3.67	0.284
N-120	5.11	3.59	0.784
N-150	4.17	3.91	0.870
N-200	5.31	-	0.510
N-250	1.54	-	0.588
N-300	4.69	-	1.342

Table 6. Deviation result of 2nd HVL's

Radiation quality	ΔHVL2 (%)		
	SSDL	***SpekCalc***	***SpekPy***
N-30	3.13	0.01	0.31
N-40	1.08	0.00	1.83
N-60	1.14	0.01	1.33
N-80	0.32	0.02	0.66
N-100	4.78	0.04	0.13
N-120	6.94	0.04	0.95
N-150	7.17	-	0.91
N-200	6.52	-	0.25
N-250	0.78	-	0.78
N-300	6.17	-	1.17

The results of the homogeneity coefficient h are in the range of 0.88 and 1 for all beam qualities, which is consistent with ISO 4037-1 for both experimental and modeled results (see Table 4).

Tables 5 and 6 show the deviations ΔHVL1(%)=|(100×[HVL1()–HVL1(ISO)]/HVL1 (ISO)|) and ΔHVL2(%) = |(100×[HVL2() – HVL2(ISO)]/HVL2(ISO)|) from the ISO 4037 standard.

The results found are all < 10% which is in agreement with the requirements of the reference X-ray field regarding the deviation of the average filter thickness from the nominal value.

3.4. X-ray Spectra

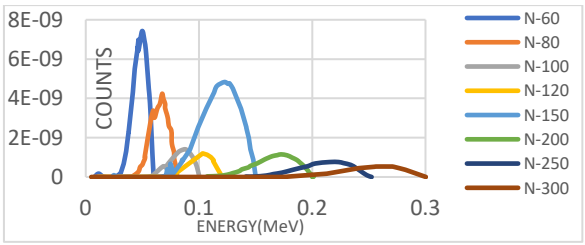

Figure 7. X-ray spectra simulated by Gamos/Geant4

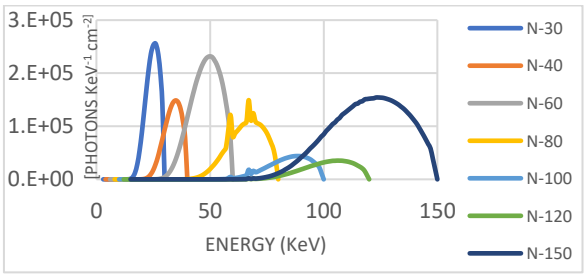

Figure 8. X-ray spectra simulated by SpekCalc

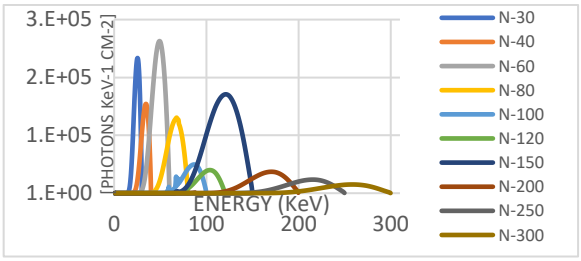

Figure 9. X-ray spectra simulated by SpekPy

Table 7. Comparison between simulated mean energies

code beams	Mean Energy (keV)			
	ISO	***Gamos/Geant4***	***Spek Calc***	***SpekPy***
N-60	47.9	47.7	48	47.61
N-80	65.2	64.6	65.6	64.93
N-100	83.3	82.57	84	82.98
N-120	100.4	100.09	101	100.03
N-150	118.2	117.4	119	117.42
N-200	164.8	162.9	-	163.66
N-250	207.3	207.1	-	207.49
N-300	248.4	248	-	249.17

Table 8. Deviation of mean energies

code beams	deviation (%)		
	ΔE_{mean} [a]	ΔE_{mean} [b]	ΔE_{mean} [c]
N-60	0.41	0.62	0.17
N-80	0.92	1.54	0.52
N-100	0.88	1.73	0.49
N-120	0.30	0.90	0.05
N-150	0.68	1.36	0.01
N-200	1.16	-	0.46
N-250	0.09	-	0.19
N-300	0.16	-	0.47

ΔE_{mean}^{a}= |100×[E_{mean}(Gamos)– E_{mean} (ISO)] / E_{mean}(ISO)|.

ΔE_{mean}^{b}=|100×[E_{mean}(SpekCalc) – E_{mean} (Gamos)/ E_{mean}(Gamos/Geant4)|.

ΔE_{mean}^{c}=|100×[E_{mean}(SpekPy) – E_{mean}(Gamos)] / E_{mean}(Gamos)|.

From Table 8 of deviation, a good agreement between simulated values of E_{mean} is noticed (maximum difference <1.16% when compared to ISO 4037-1 data, <1.73% when compared to SpekCalc data, and 0.52% when compared to SpekPy).

3.5. Conversion coefficients

Table 9. Conversion coefficients from air kerma to dose equivalent at 10 mm depth

hpK(10;N,α) in Sv/Gy						
Angle of incidence	***N-60***		***N-80***		***N-100***	
	Experiment	***ISO***	***Experiment***	***ISO***	***Experiment***	***ISO***
0°	1.64	1.66	1.89	1.89	1.88	1.88
15°	1.64	1.64	1.88	1.87	1.87	1.87
30°	1.59	1.6	1.8	1.83	1.86	1.82
45°	1.42	1.49	1.76	1.72	1.79	1.73
60°	1.3	1.29	1.52	1.51	1.48	1.53
75°	0.8	0.86	1	1.07	1.02	1.12

Table 9. Continued

Angle of incidence	N-150		N-250	
	Experiment	ISO	Experiment	ISO
0°	1.71	1.72	1.49	1.48
15°	1.71	1.71	1.48	1.47
30°	1.67	1.68	1.47	1.46
45°	1.56	1.61	1.44	-
60°	1.38	1.46	1.36	1.33
75°	1	1.1	1	1.08

Table 10. Comparison between experimental conversion coefficients and reference values (%)

Angle of incidence	ΔhpK((10;N,α) (%)				
	N-60	N-80	N-100	N-150	N-250
0°	1.20	0	0	0.58	0.68
15°	0	0.53	0	0	0.68
30°	0.62	1.64	2.2	0.6	0.69
45°	4.7	2.31	3.47	3.10	-
60°	0.8	0.66	3.27	5.48	2.26

ΔhpK((10;N,α)=|100*hpk(experimental)-hpk(refrence) /hpk(reference)|.

At different angles (0°, 15°, 30°, 45°, and 60°), the conversion coefficients for the ISO narrow spectrum series were calculated and compared to the reference values (ISO 4037). Table 9 provides a summary of the results, and Table 10 compares experimental, and reference values. The highest difference between the conversion coefficients determined through experiment and those established by ISO 4037-3 is 5.5 %. This can be explained by the possibility that at 150 kV, the photons dispersed by the Compton effect at this angle of 60 degrees may have high secondary electron energies and no longer attain electronic equilibrium.

These outcomes can be regarded as totally satisfactory.

4. Conclusion

This work presented the procedure applied for the determination of the characteristics recommended by the ISO 4037 standard to establish the standard radiation qualities designed for the calibration of radiation protection instruments.

The results obtained for the (1st HVL) and the (2nd HVL) are all in agreement with the of the ISO 4037 standard. In addition, the generation of the spectral features was performed using the Gamos/Geant4 Monte Carlo code. The X-ray spectra produced have average energy in agreement with those of the reference radiations given by the ISO standard and found by the SpekPy and SpekCalc validation software. Moreover, the experimentally determined conversion coefficients for the personal dose equivalent Hp(10) are consistent with the ISO 4037-3 standard values which reflects the high-quality metrology of this system [22].

Therefore, the national secondary dosimetry laboratory (SSDL) of Morocco, which is a member of the WHO/IAEA network can irradiate samples for internal studies and the N-quality could be used in the SSDL for the calibration of different dosimeters [32,33].

Declaration of competing interest. *The authors declare that they have no known competing financial interests or personal relationships that could have appeared to influence the work reported in this paper.*

Acknowledgments: *This research was supported through computational resources of HPC-MARWAN (www.marwan.ma/hpc) provided by the National Center for Scientific and Technical Research (CNRST), Rabat, Morocco.*

References

1. *Radiological protection — X and gamma reference radiation for calibrating dosemeters and doserate meters and for determining their response as a function of photon energy — Part 1: Radiation characteristics and production methods*, ISO 4037-1:2019, Jan. 1, 2019. Retrieved from: https://www.iso.org/standard/66872.html Retrieved on: Jun. 1, 202
2. *Radiological protection — X and gamma reference radiation for calibrating dosemeters and doserate meters and for determining their response as a function of photon energy — Part 2: Dosimetry for radiation protection over the energy ranges from 8 keV to 1,3 MeV and 4 MeV to 9 MeV*, ISO 4037-2:2019, Jan. 1, 2019. Retrieved from: https://www.iso.org/standard/66873.html Retrieved on: Jun. 1, 2022
3. *Radiological protection — X and gamma reference radiation for calibrating dosemeters and doserate meters and for determining their response as a function of photon energy — Part 3: Calibration of area and personal dosemeters and the measurement of their response as a function of energy and angle of incidence*, ISO 4037-3:2019, Jan. 1, 2019. Retrieved from: https://www.iso.org/standard/66874.html Retrieved on: Jun. 1, 2022
4. *Radiological protection — X and gamma reference radiation for calibrating dosemeters and doserate meters and for determining their response as a function of photon energy — Part 4: Calibration of area and personal dosemeters in low energy X reference radiation fields*, ISO 4037-4:2019, Jan. 1, 2019. Retrieved from: https://www.iso.org/standard/66165.html Retrieved on: Jun. 1, 2022
5. D. Kurkova, L. Judas, "X-ray tube spectra measurement and correction using a CdTe detector and an analytic response matrix for photon energies up to 160 keV," *Radiation Measurements*, vol. 85, pp. 64–72, Feb. 2016. https://doi.org/10.1016/j.radmeas.2015.12.008
6. Physical aspects of irradiation: recommendations of the International Commission on Radiological Units and Measurements (ICRU), Report 10b, National Bureau of Standards – Handbook 85, Washington (DC), USA, 1964. Retrieved from: https://nvlpubs.nist.gov/nistpubs/Legacy/hb/nbshandbook85.pdf Retrieved on: Jun. 5, 2022
7. G. Poludniowski, P. Evans, "Calculation of x-ray spectra emerging from an x-ray tube. Part I. electron penetration characteristics in x-ray target," *Med. Phys.*, vol. 34, no. 6, part 1, pp. 2164–2174, Jun. 2007. https://doi.org/10.1118/1.2734725
8. G. Poludniowski, "Calculation of x-ray spectra emerging from an x-ray tube. Part II. X-ray production and filtration in x-ray targets," *Med. Phys.*, vol. 34, no. 6, part 1, pp. 2175–2186, Jun. 2007. https://doi.org/10.1118/1.2734726
9. G. Poludniowski, G. Landry, F. DeBlois, P. M. Evans, F. Verhaegen, "SpekCalc: a program to calculate photon

spectra from tungsten anode x-ray tubes," *Phys. Med. Biol.*, vol. 54, no. 19, pp. 433–438, Sep. 2009. https://doi.org/10.1088/0031-9155/54/19/n01
10. G. Poludniowski, A. Omar, R. Bujila, P. Andreo, "Technical Note: SpekPy v2.0—a software toolkit for modeling x-ray tube spectra," *Med. Phys.*, vol. 48, no. 7, pp. 3630–3637, Jul. 2021. https://doi.org/10.1002/mp.14945
11. R. Bujila, A. Omar, G Poludniowski, "A validation of SpekPy: A software toolkit for modelling X-ray tube spectra," *Phys. Med.*, vol. 75, pp. 44–54, Jul. 2020. https://doi.org/10.1016/j.ejmp.2020.04.026
12. A. Omar, P. Andreo, G. Poludniowski, "A model for the energy and angular distribution of x rays emitted from an x-ray tube. Part I. Bremsstrahlung production," *Med. Phys.*, vol. 47, no. 10, pp. 4763–4774, Oct. 2020. https://doi.org/10.1002/mp.14359
13. A. Omar, P. Andreo, G. Poludniowski, "A model for the energy and angular distribution of x rays emitted from an x-ray tube. Part II. Validation of x-ray spectra from 20 to 300 kV," *Med. Phys.*, vol. 47, no. 9, pp. 4005–4019, Sep. 2020. https://doi.org/10.1002/mp.14360
14. A. Omar, P. Andreo, G. Poludniowski, "A model for the emission of K and L x rays from an x-ray tube," *Nuclear Instruments and Methods in Physics Research Section B: Beam Interactions with Materials and Atoms*, vol. 437, pp. 36–47, Dec. 2018. https://doi.org/10.1016/j.nimb.2018.10.026
15. G. Poludniowski, "Calculation of x-ray spectra emerging from an x-ray tube. Part II. X-ray production and filtration in x-ray targets," *Med. Phys.*, vol. 34, no. 6, pp. 2175–2186, Jun. 2007. https://doi.org/10.1118/1.2734726
16. G. Poludniowski, P. Evans, "Calculation of x-ray spectra emerging from an x-ray tube. Part I. Electron penetration characteristics in x-ray targets," *Med. Phys.*, vol. 34, no. 6, part 1, pp. 2164–2174, Jun. 2007. https://doi.org/10.1118/1.2734725
17. G. Poludniowski, G. Landry, F. DeBlois, P. Evans, F. Verhaegen, "*SpekCalc*: a program to calculate photon spectra from tungsten anode x-ray tubes," *Phys. Med. Biol.*, vol. 54, no. 19, article no. 433, Sep. 2009. https://doi.org/10.1088/0031-9155/54/19/N01
18. A. Omar, P. Andreo, G. Poludniowski, "Performance of different theories for the angular distribution of bremsstrahlung produced by keV electrons incident upon a target," *Radiat. Phys. Chem.*, vol. 148, pp. 73–85, Jul. 2018. https://doi.org/10.1016/j.radphyschem.2018.02.009
19. P. Arce, P. Rato, M. Canadas, J. I. Lagares, "GAMOS: A GEANT4-based easy and flexible framework for nuclear medicine applications," in Proc. *IEEE Nuclear Science Symposium Conference Record*, Dresden, Germany, 2008, pp. 3162–3168. https://doi.org/10.1109/NSSMIC.2008.4775023
20. O. E. Belhaj, H. Boukhal, E. M. Chakir, "Monte Carlo and Medical Physics," in *The Monte Carlo Methods - Recent Advances, New Perspectives and Applications*, A. A. Jaoudé, Ed., London, UK: IntechOpen, 2021, ch. 5, pp. 155–176. https://doi.org/10.5772/intechopen.100121
21. I. Kawrakow, E. Mainegra-Hing, D.W.O. Rogers, F. Tessier, B.R.B. Walters, *The EGSnrc Code System: Monte Carlo Simulation of Electron and Photon Transport*, NRCC Report PIRS–701, National Research Council of Canada, Ottawa, Canada, 2000. Retrieved from: https://nrc-cnrc.github.io/EGSnrc/doc/pirs701-egsnrc.pdf Retrieved on: April 15, 2021
22. W. R. Nelson, H. Hirayama, D. W. O. Rogers, *The EGS4 code system*, Report SLAC–265, Stanford Linear Accelerator Center, Menlo Park (CA), USA, 1985. Retrieved from: https://www.osti.gov/biblio/6137659 Retrieved on: April 15, 2021
23. L. Zhe et al., "Establishment of radiation in (10-40) kV narrow spectrum series," in Proc. *14th IEEE Int. Conf. Electron. Meas. Instr. (ICEMI 2019)*, Changsha, China, 2019, pp. 1454–1459. https://doi.org/10.1109/ICEMI46757.2019.9101438
24. S. M. Seltzer, "An overview of ETRAN Monte Carlo methods," In *Monte Carlo Transport of Electrons and Photons,* T. M. Jenkins, W. R. Nelson, A. Rindi, Eds., Ettore Majorana International Science Series vol. 38, New York (NY), USA: Springer-Plenum Press, 1988, ch. 7, pp. 153–182. https://doi.org/10.1007/978-1-4613-1059-4_7
25. *MCNP—A general Monte Carlo N-particle transport code, Version 5 - Volume 1: Overview and theory*, Report LA-UR-03-1987, Los Alamos National Laboratory, Los Alamos (NM), USA, 2003. Retrieved from: https://mcnp.lanl.gov/pdf_files/TechReport_2003_LANL_LA-UR-03-1987Revised212008_SweezyBoothEtAl.pdf Retrieved on: Aug. 2, 2022
26. *PENELOPE-2006: A Code System for Monte Carlo Simulation of Electron and Photon Transport*, Nuclear Energy Agency, Paris, France: OECD Publishing, 2006. Retrieved from: https://www.oecd-nea.org/upload/docs/application/pdf/2019-12/nea6222-penelope.pdf Retrieved on: Jul. 7, 2022
27. R. Taleei, M. Shahriari, "Monte Carlo simulation of X-ray spectra and evaluation of filter effect using MCNP4C and FLUKA code," *Applied Radiation and Isotopes*, vol. 67, no. 2, pp. 266–271, Feb. 2009. https://doi.org/10.1016/j.apradiso.2008.10.007
28. A. Arectout et al., "Calculation of X-ray spectra characteristics and kerma to personal dose equivalent $H_p(10)$ conversion coefficients: Experimental approach and Monte Carlo modeling," *Nucl. Eng. Technol.*, vol. 54, no. 1, pp. 301–309, Jan. 2022. https://doi.org/10.1016/j.net.2021.07.028
29. R. Antoni, L. Bourgois, *Physique appliquée à l' exposition externe. Dosimétrie et radioprotection*, París, France: Springer,2012. (R. Antoni, L. Bourgois, *Physics applied to external exposure. Dosimetry and radiation protection*, France: Paris, France: Springer, 2012.) https://doi.org/10.1007/978-2-8178-0311-1
30. *Detectors for Ionizing Radiation, Including Codes of Practice*, Detector Catalog, PTW, Freiburg, Germany, 2013. Retrieved from: http://www.ptw.de/online_brochures.html Retrieved on: Aug. 5, 2022
31. S. Principi, C. Guardiola, M. A. Duch, M. Ginjaume, "Air kerma to H_p (3) conversion coefficients for IEC 61267 RQR X-ray radiation qualities: Application to dose monitoring of the lens of the eye in medical diagnostics," *Radiation Protection Dosimetry*, vol. 170, no. 1–4, pp. 45–48, Sep. 2016. https://doi.org/10.1093/rpd/ncv435
32. N. Melhem, H. El Balaa, G. Younes, Z. Al Kattar, "Characteristics of the narrow spectrum beams used in the Secondary standard dosimetry laboratory at the Lebanese atomic energy commission," *Radiation Protection Dosimetry*, vol. 175, no. 2, pp. 252–259, Jun. 2017. https://doi.org/10.1093/rpd/ncw293
33. O. E. Belhaj et al., "Dose metrology: TLD/OSL dose accuracy and energy response performance," *Nuclear Engineering and Technology*, accepted for publication. https://doi.org/10.1016/j.net.2022.10.029